

Decoherence in semiconductor nanostructures with type-II band alignment: All-optical measurements using Aharonov-Bohm excitons

I. L. Kuskovsky,^{1,2} L. G. Mourokh,^{1,2} B. Roy,^{1,2} H. Ji,^{1,2} S. Dhomkar,^{1,2} J. Ludwig,^{3,4} D. Smirnov,^{3,4} and M. C. Tamargo^{2,5}

¹*Department of Physics, Queens College of The City University of New York (CUNY), Flushing, New York 11367, USA*

²*The Graduate Center of CUNY, New York, New York 10016, USA*

³*National High Magnetic Field Laboratory, Tallahassee, Florida 32310, USA*

⁴*Department of Physics, Florida State University, Tallahassee, Florida 32306, USA*

⁵*Department of Chemistry, The City College of CUNY, New York, New York 10031, USA*

(Received 30 May 2015; revised manuscript received 1 January 2017; published 26 April 2017)

We examine the temperature dependence of the visibility of the excitonic Aharonov-Bohm peak in type-II quantum dots. We obtain a functional temperature dependence that is similar to that determined by transport experiments, namely, with the T^{-1} term due to electron-electron collisions and the T^{-3} term due to electron-phonon interactions. However, the magnitude of the latter term is much smaller than that for the transport electrons and similar to the interaction strength of the exciton-phonon coupling. Such suppressed electron-phonon interaction ushers a way for all-optical studies of decoherence processes in semiconductor nanostructures as other dephasing mechanisms become more pronounced.

DOI: [10.1103/PhysRevB.95.165445](https://doi.org/10.1103/PhysRevB.95.165445)

I. INTRODUCTION

Understanding the mechanisms of decoherence processes at the nanoscale has been a focus of research over the last 30 years. These studies are important from a fundamental point of view, because such processes lead to a crossover between quantum and classical regimes, as well as due to the need to understand the behavior of modern nanoscale optoelectronic devices. For a long time, the main advances in this field have been associated with the observations of various quantum-mechanical phenomena in transport experiments in mesoscopic metals and semiconductors (e.g., [1,2]), such as weak localization and antilocalization, universal conductance fluctuations, Aharonov-Bohm (AB) oscillations, and persistent currents. From these experiments, decoherence length (and time) can be extracted and compared to theoretical predictions.

According to pioneering papers [3,4], the main decoherence mechanisms in mesoscopic systems are the electron-phonon (e-ph) and electron-electron (ee) interactions, with the temperature dependence of the inverse phase-breaking time given by

$$\tau_{\phi}^{-1} = \tau_{ee}^{-1} + \tau_{e-ph}^{-1} = aT^n + bT^3, \quad (1)$$

where generally $n = 2/3$ [3,4] for nanowires and $n = 1$ for AB rings (e.g., Refs. [5–7] and references therein) in the diffusive regime; in the ballistic one-channel regime, the dephasing length and time were shown to behave as T^{-1} (e.g., Refs. [8,9]). In both cases the dephasing time is expected to diverge as $T \rightarrow 0$; however, in many actual experiments starting from Ref. [10] (for reviews, see Refs. [11,12] and references therein), the dephasing time *saturates* at very low temperatures.

In the present paper, we propose measurements of decoherence in semiconductors using a *contactless all-optical* experimental technique. Our paper is based on the excitonic Aharonov-Bohm effect (EABE) in type-II quantum dots (QDs). It was predicted that a nontrivial quantum phase can be acquired by an electric dipole moving in a magnetic field [13–16], and it can be observed via optical emission of radially polarized excitons in nanostructures with suitable ringlike geometry, such as quantum rings and type-II disklike QDs

(e.g., [15–18]). The EABE has been experimentally observed in a number of type-II QD systems by us and other groups, in quantum rings (Ref. [19] and references therein), as well as in type-I QDs with a suitable quantum well geometry [20]. Optical experiments are advantageous over conventional transport experiments for a number of reasons. First, they are contactless, so the account of contacts and contact configuration can be eliminated. Many efforts have been exerted previously to include contacts and their configurations in both analyses of experimental results and theoretical considerations [2,5,21–23]. Second, the EABE peak [24] is observed at a sufficiently large magnetic field (see Fig. 1 and discussion below), where the scattering on magnetic impurities, if any, is strongly suppressed [12,25–27]. Third, as we show below, the inelastic interactions with phonons are much weaker for the light-excited electron-hole pairs than for the electrons participating in transport, so other dephasing mechanisms, such as pure dephasing and electron-impurity scattering, become more pronounced.

The rest of the paper is structured as follows. We present experimental data in Sec. II. In Sec. III, we examine theoretically the type-II exciton with weak electron-hole bonding and conclude that such a system would *not* reproduce the observed features. Correspondingly, experimental results are discussed in Sec. IV from the point of view of the strongly-bound model. The paper is summarized in Sec. V.

II. EXPERIMENTAL RESULTS

The samples studied are type-II ZnTe/ZnSe stacked submonolayer QDs grown using a combination of migration-enhanced epitaxy and molecular beam epitaxy (see Refs. [28–30] and references therein). The stacks are formed due to a strong vertical correlation between the QD-containing layers [31,32]. The lateral separation between the QD stacks is much larger [33] than the size of the carrier orbit [34], allowing for the assumption that carriers orbit each stack independently. There are no magnetic impurities expected in these samples due to the nature of the growth procedure.

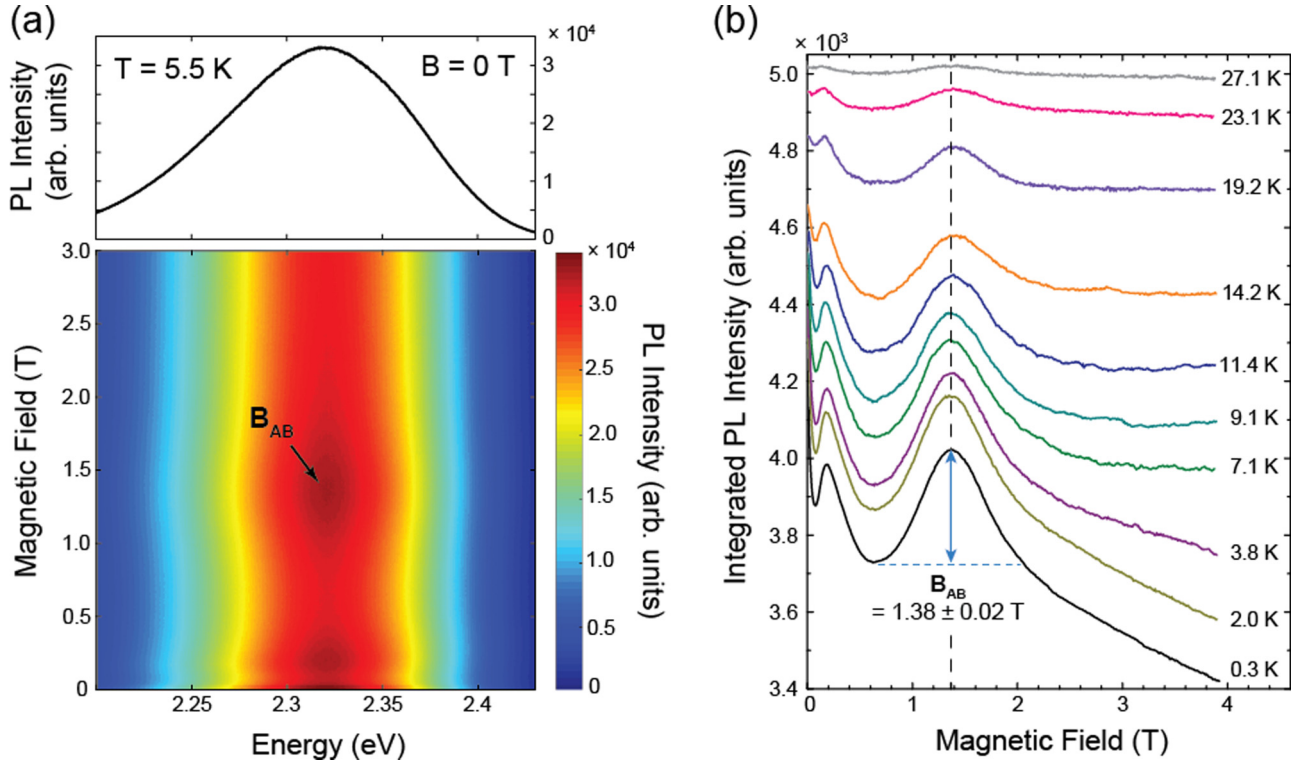


FIG. 1. (a) Photoluminescence of a sample with type-II QDs at a zero magnetic field. (b) Magneto-PL of the same sample at the same temperature with magnetic fields up to 4 T; the peak at ~ 1.38 T is due to EABE. (c) Integrated PL as a function of the magnetic field at different temperatures. Note: The plots are not shifted; rather, they show actual experimental values.

Magnetophotoluminescence (magneto-PL) measurements were performed at temperatures between 0.36 and 30 K, with magnetic fields up to 18 T applied in the Faraday geometry using a high-field magneto-optical insert, as described in Ref. [35]. Light from a ThorLabs temperature-controlled 405 nm laser diode was injected into a 365 μm fiber and delivered to the sample in a ^3He cryostat. Optical power density across the excitation spot was fixed to $\sim 10 \mu\text{W}/\text{cm}^2$. The collected photoluminescence (PL) was injected into a 550 μm fiber and delivered to a Princeton Instruments IsoPlane single grating spectrometer equipped with a thermoelectrically cooled charge-coupled device (CCD) detector.

In Fig. 1(a), we show PL spectrum at 5.5 K and zero magnetic field for one of the samples studied, whereas Fig. 1(b) shows the corresponding magneto-PL up to 4 T for the same sample. This sample exhibits emission due to QDs only (see, e.g., Refs. [30,33] for PL from a set of samples that have both QD and isoelectronic bound exciton related emission), which allows for simple spectral integration. The result is shown in Fig. 1(b). The signal persists to above 27 K, indicating that the effect is very robust, which allows one to perform decoherence measurements by varying the temperature over two orders of magnitude. The peak (henceforth called the AB peak) at $B_{\text{AB}} \sim 1.38$ T is due to EABE [36]. The exact position of the peak changes slightly with temperature for this sample; however, considering that we plot the AB transition from an integrated PL intensity rather than over a specific spectral position, it is not unexpected and does not affect the magnitude of the AB peak. The magnitude of the AB peak [30], counted from the minima for each curve, as shown by the arrow in

Fig. 1(b) for the 0.3 K curve, and is plotted as a function of temperature in Fig. 2 (solid circles). The magnitude of the AB peak directly relates to the coherence of the carriers responsible for the optical emission.

III. WEAKLY- VERSUS STRONGLY-BOUND EXCITONS: THEORETICAL EXAMINATION

To further analyze the observed behavior, one needs to understand the type (strength) of the electron-hole interaction,

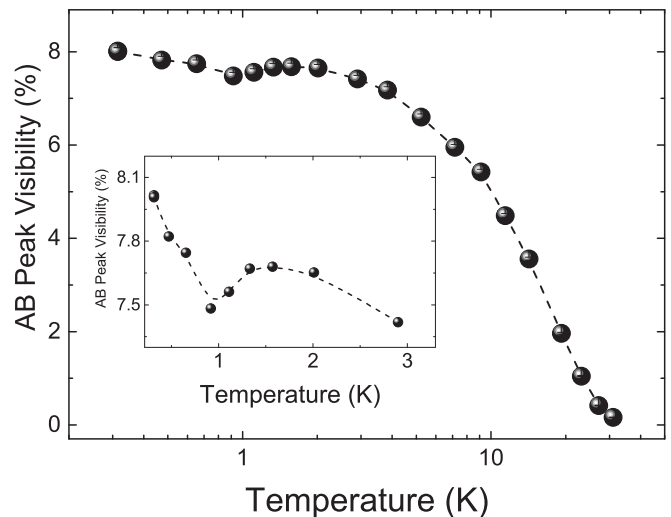


FIG. 2. Magnitude of the AB peak as a function of temperature. The dashed line is for visual guidance only.

which determines the character and shape of the optical AB peak. Two possible cases are discussed in Ref. [18]. For the weakly-bound exciton, when the electron and hole move independently, the exciton energy is given by

$$E_{\text{exc}}^{\text{wb}} = E_g^{\text{wb}} + E_e + E_h, \quad (2)$$

where E_g^{wb} is the magnetic-field-independent term,

$$E_e = \frac{\hbar^2}{2m_e R_e^2} \left(l_e + \frac{\Phi_e}{\Phi_0} \right)^2, \quad (3)$$

$$E_h = \frac{\hbar^2}{2m_h R_h^2} \left(l_h - \frac{\Phi_h}{\Phi_0} \right)^2, \quad (4)$$

$m_{e(h)}$ is the electron (hole) effective mass, $R_{e(h)}$ is the radius of the electron (hole) trajectory, $l_{e(h)}$ is the electron (hole) angular momentum, and $\Phi_{e(h)}$ is the magnetic flux through electron (hole) closed path loop. At zero magnetic field, the ground state is a bright state with $(l_e, l_h) = (0, 0)$. With increasing magnetic field, eventually the dark state $(l_e, l_h) = (-1, 0)$ becomes the ground one. However, for certain geometries, further increase of the magnetic field can make the ground state bright with $(l_e, l_h) = (-1, +1)$ and dark again with $(l_e, l_h) = (-2, +1)$. In this case, the enhancement of the luminescence is caused by the reappearance of the bright exciton. The corresponding luminescence peak position, width, and shape are determined mainly by the system geometry. Moreover, the second peak associated with the bright state $(l_e, l_h) = (-2, +2)$ can occur.

For the tightly-bound exciton, when the electron and hole move together, the exciton energy is given by

$$E_{\text{exc}}^{\text{tb}} = E_g^{\text{tb}} + E_{e-h}, \quad (5)$$

where E_g^{tb} is the magnetic-field-independent term,

$$E_{e-h} = \frac{\hbar^2}{2MR_0^2} \left(L + \frac{\Delta\Phi}{\Phi_0} \right)^2, \quad (6)$$

$R_0 = (R_e + R_h)/2$, $M = (m_e R_e^2 + m_h R_h^2)/R_0^2$, $L = l_e + l_h$, and $\Delta\Phi$ is the net magnetic flux through the area between the electron and hole trajectories. With such strongly correlated motion, the ground-state momentum only increases with magnetic field and the bright state cannot reappear. In this case, the luminescence can be enhanced when the energies of the states with $L = 0$ and $L = +1$ become degenerated. In the ideal situation, there is just the level crossing. However, in reality, these states can be mixed (in particular, via the spin-orbit interaction) leading to the appearance of the two partially-bright states and possible enhancement of the luminescence. The experimentally obtained position of the peak does not allow one to choose one model vs the other. However, the predictions for a peak width and its shape are very different for each model.

For the case of the weakly-bound exciton, the magnitude of the peak can be affected by temperature via thermal broadenings of the levels. The temperature dependence of the visibility can be estimated from the contributions of the bright exciton populations. If the populations of the electron and hole levels are proportional to the Boltzmann factors, as

$$N_i^{e,h} \propto \exp \left\{ -\frac{E_i^{e,h}}{k_B T} \right\}, \quad (7)$$

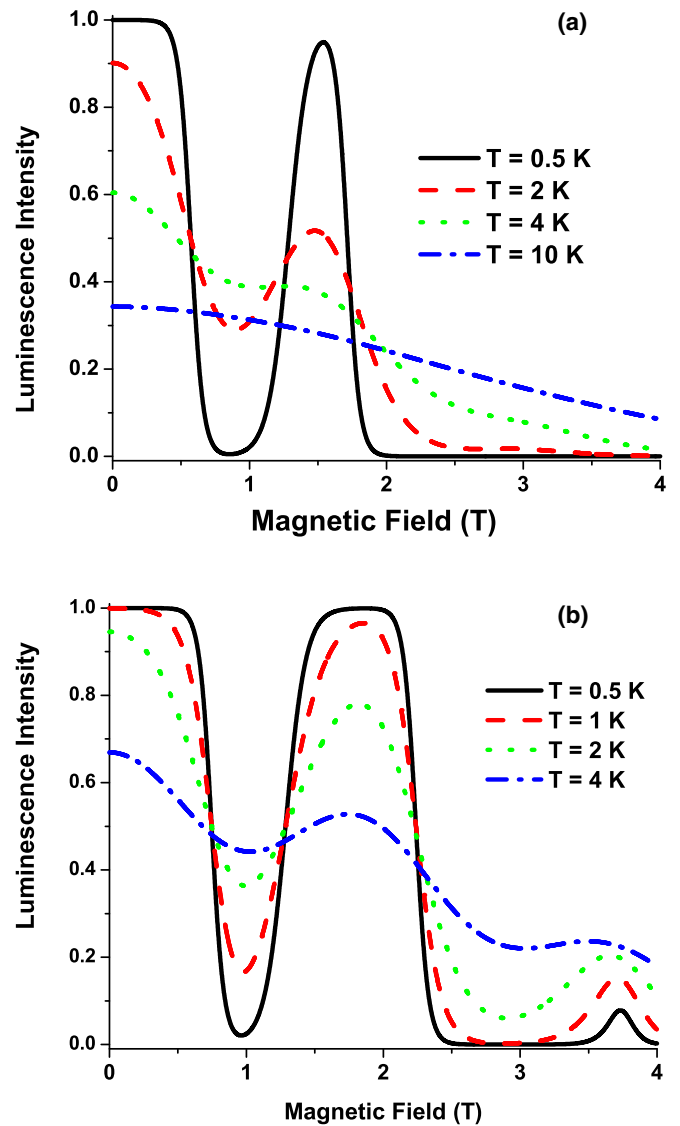


FIG. 3. Calculated relative intensity of the luminescence as a function of magnetic field for various temperatures in the case of weakly-bound excitons. (a) $R_h = 16$ nm, $R_e = 24$ nm; (b) $R_h = 16$ nm, $R_e = 21$ nm.

where $E_i^{e,h}$ are the electron and hole energies from Eqs. (3) and (4) with angular momenta $i = 0, \pm 1, \pm 2, \dots$, then the luminescence intensity is given by

$$I = \frac{\sum N_i^e N_{-i}^h}{\sum N_i^e \sum N_i^h}. \quad (8)$$

The dependence of this intensity on the applied magnetic field is shown in Fig. 3 for various temperatures.

It is evident from this figure that the width and shape of the peak differ drastically from the experiment. Moreover, a slight change of the system parameters can lead to the appearance of the second peak, as can be seen from Fig. 3(b). The samples are evidently different from each other; nevertheless, we have not observed a clear peak at the double magnetic field value at lower temperatures. The corresponding temperature dependence of the visibility is shown in Fig. 4. One can see that while the magnitude of the peak does indeed go down with

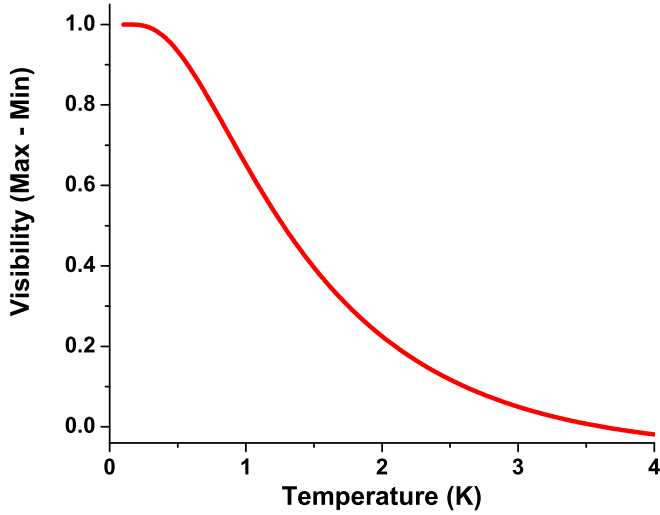


FIG. 4. Calculated temperature dependence of the visibility in the case of weakly-bound excitons.

temperature as a result of thermal broadening, the functional dependence is different from the experimental results (Fig. 2). Moreover, the peak completely disappears above 4 K, which is in contradiction to our observations.

All these facts allow us to rule out the model of the weakly-bound (independent) electron-hole pair for our structures. For the tightly-bound excitons, thermal broadening would not affect the peak magnitude, although can be responsible for the initial luminescence suppression with the increasing magnetic field. The arguments based on the comparison of the observed AB exciton size and the free excitons in ZnSe and ZnTe also led to the tight-binding model [37]. Moreover, we point to recent high resolution x-ray diffraction (HRXRD) measurements on the same sample [32] that gave the average size of these QDs of 16 to 23 nm in radius, in excellent agreement with the tight-binding model [37].

IV. DISCUSSION

We thus believe that the temperature effects on the visibility are produced by the loss of coherence, i.e., by the destruction of the states with a well-defined angular momentum. In our model, therefore, while an electron and a hole are strongly coupled to form an exciton [33,37], the electron travels over longer distances outside of the dot than the confined hole and its probability to be scattered is much larger. Correspondingly, the magnitude of the AB peak decreases exponentially with the electron path length D , similar to the amplitude of the AB oscillations observed in transport measurements (e.g., Refs. [9,38] and references therein): $\Delta I_{AB} \propto \exp[-D/D_\phi]$, where D_ϕ is the coherence length. We also assume here that the ballistic regime applies so that $D_\phi \propto \tau_\phi$. Indeed, as stated above, the lateral electron trajectory radius R_{QD} of the dots in all of our samples is between 15 and 30 nm [34,37], resulting in an electron path around the QD stacks, $2\pi R_{QD}$, between 100 and 200 nm. Thus, for further analyses, we assume

$$\Delta I_{AB} \propto \exp\left[-\frac{t_0}{\tau_\phi}\right], \quad (9)$$

TABLE I. The fitting parameters to Eq. (10) for the experimental data of three samples.

Sample	$At_0(\text{K}^{-1}), 10^{-2}$	$bt_0(\text{K}^{-3}), 10^{-5}$
D47	4	9.2
D51	2.9	2.5
D55	6.7	4.6

where t_0 is the time an exciton spends on the orbit before recombining *either radiatively or nonradiatively*, similar to the time an electron spends in an interferometer or an AB ring in transport experiments [7]. Therefore, the experimental data are analyzed with the help of the following expression:

$$\Delta I_{AB} = \Delta I_{AB}(0) \Delta \exp[-At_0T - bt_0T^3]. \quad (10)$$

The result of fitting the experimental data to Eq. (10) is shown in Fig. 3 (red dashed line); the best fit was obtained for $At_0 = 0.04 \text{ K}^{-1}$ and $bt_0 = 9.2 \times 10^{-5} \text{ K}^{-3}$. The values for the other samples are shown in Table I. We also show in Fig. 5 the separated best fits for the dependence of decoherence time for low (T^{-1}) and high temperature (T^{-3}) cases. It is obvious that both the electron-electron-like and the electron-phonon-like scattering mechanisms must be included.

Next, we point out that in optical emission experiments, t_0 corresponds to the average lifetime of the electrons, as measured by PL decay, and accounts for both radiative and nonradiative recombinations. In our samples, within the temperature range of this experiment, the average PL lifetime was determined to be between 50 and 100 ns [33]. This allows us to estimate $A = (4 \div 8) \times 10^{-4} \text{ ns}^{-1} \text{ K}^{-1}$ and $b = (9.2 \div 18.4) \times 10^{-7} \text{ ns}^{-1} \text{ K}^{-3}$. It should be emphasized that the value of parameter b here is much smaller than the approximately $5 \times 10^{-3} \text{ ns}^{-1} \text{ K}^{-3}$ obtained after introducing ZnSe parameters into the corresponding expression in Ref. [39], where electron-phonon effects on decoherence were addressed. To further stress this point, we estimate parameter b , assuming that decoherence occurs via strictly nonradiative recombination even though one would expect the quenching of the overall PL as well, which we do not observe. The

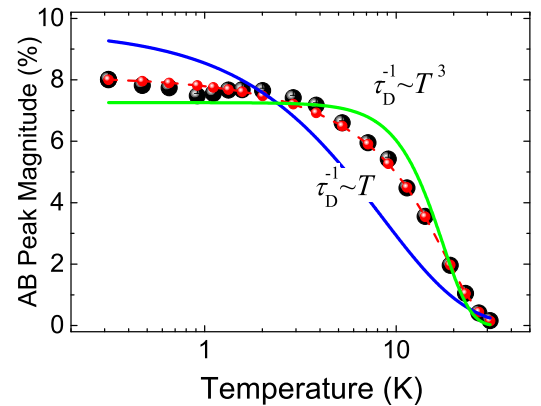


FIG. 5. Magnitude of the AB peak as a function of the temperature. The red dashed line is the fit to the functional dependence that accounts for electron-phonon and electron-electron scattering [Eq. (10)]. Solid lines (green and blue) show dependencies arising from each mechanism, separately.

nonradiative times estimated in Ref. [33] are of the order of 0.1–1 ns and would give a parameter b of $\sim 10^{-3}$ to 10^{-4} , which is still at least a factor of 5 smaller.

We attribute the smallness of parameter b to a strong electron-hole coupling due to an electrostatic interaction that cannot be neglected in type-II QDs [24]. Thus, even when only the electron is scattered, the whole electron-hole system emits or absorbs phonons, which diminishes such an energy exchange. The situation here is similar to the phonon scattering by donor-bound electrons considered by Kwok [40] for germanium. In our case, the confined hole plays the role of the positively charged donor. It was shown that the electron-phonon interaction is affected because of the discrete electron excitation spectrum. For the nonresonant case, the matrix element of the interaction can be calculated using second-order Born perturbation theory; i.e., it is strongly suppressed. We further note that parameter b is of the same order for all the samples we have measured, which indicates the material-fundamental and sample-independent character of the exciton-phonon interaction.

In Ref. [41], the temperature dependence of the excitonic dephasing rate was determined for temperatures from 5 to 120 K by means of the four-wave mixing technique. The authors obtained a good fit using the predictions of the modified independent boson model [42] for the decoherence rate as

$$\gamma = \gamma_0 + \alpha T + b_1 \frac{1}{e^{E_1/k_B T} - 1} + b_2 \frac{1}{e^{E_2/k_B T} - 1}. \quad (11)$$

Here, E_1 and E_2 are the activation energies, with one of the energies (the larger one) being the optical phonon energy. The origin of the smaller energy was not well discussed, and the possibility of pure dephasing was not excluded. Our attempt to fit our data using Eq. (11) resulted in two very similar values for the activation energy in the range of 2 to 6 meV, indicating that the interaction with optical phonons is not a decoherence mechanism for the AB excitons discussed here, in contrast to the results of Ref. [41], as expected for the temperature range below 30 K that is investigated here. Moreover, the α parameter of Eq. (11) was determined to be zero in Ref. [41], indicating completely different functional temperature dependencies.

We attribute this difference to the fact that in type-I QDs of Ref. [41] both electrons and holes are confined, whereas in our type-II QD system electrons are mobile and thus scattered as in transport experiments. Correspondingly, we have to conclude that the phonon-induced dephasing in our system is due to *electron-acoustic-phonon* scattering, however, with

diminished magnitude because of the strong electron-hole coupling [40].

Finally, we comment on the low temperature data shown in the inset of Fig. 2, which indicate the existence of a minimum in the magnitude of the AB peak at around 1 K for this particular sample. We also observed smaller dips in other samples and somewhat different temperatures but within the same overall temperature range. The nature of this dip is not completely understood at this time, but it can be attributed to changes in the overall PL intensity observed from the samples. We plan to investigate it further, but we believe that it does not affect the overall temperature dependence of the AB peak presented in this paper because our fitting covers a much larger temperature range than the dip vicinity.

V. SUMMARY

We proposed a way to determine the temperature dependences of decoherence mechanisms based on an all-optical technique. The strength of the EABE was measured as a function of temperature over two orders of magnitude. We showed that at temperatures above 3 K, exciton-phonon scattering is the dominant cause of decoherence and is the same for all samples. The obtained functional dependence on temperature is in agreement with that obtained in the electron transport experiments, but the magnitude of the decoherence rate is much smaller, confirming the benefits of the optical measurements.

ACKNOWLEDGMENTS

The paper is supported by the National Science Foundation (NSF) under Award No. DMR-1006050 and the U.S. Department of Energy (DOE), Office of Basic Energy Sciences, Division of Materials Sciences and Engineering under Award No. DE-SC003739. Sample preparation was carried out with the DOE support (S.D., M.C.T., and I.L.K.), while optical investigations were performed with the support from the NSF (H.J. and I.L.K.). J.L. and D.S. acknowledge support by National High Magnetic Field Laboratory (NHMFL) User Collaboration Grants Program (UCGP) No. 5087. The work of L.M. is partially supported by the Air Force Office of Scientific Research (AFOSR) under Award No. FA9550-16-1-0279. A portion of this work was performed at the NHMFL, which is supported by NSF Cooperative Agreement No. DMR-1157490 and the State of Florida.

-
- [1] Y. Imry, in *Introduction to Mesoscopic Physics, Mesoscopic Physics and Nanotechnology Series, Book 2* (Oxford University Press, New York, 2002), p. 256.
- [2] T. Ihn, in *Electronic Quantum Transport in Mesoscopic Semiconductor Structures* (Springer-Verlag, New York, 2004), Vol. 192, p. 270.
- [3] B. L. Altshuler, A. G. Aronov, and D. Khmel'nitskii, *J. Phys. C* **15**, 7367 (1982).
- [4] B. L. Altshuler and A. G. Aronov, in *Electron-Electron Interaction in Disordered Systems*, edited by A. L. Efros and M. Pollak (North Holland, Amsterdam, 1985), p. 1.
- [5] T. Capron, C. Texier, G. Montambaux, D. Mailly, A. D. Wieck, and L. Saminadayar, *Phys. Rev. B* **87**, 041307 (2013).
- [6] T. Ludwig and A. D. Mirlin, *Phys. Rev. B* **69**, 193306 (2004).
- [7] T. Ihn, in *Semiconductor Nanostructures: Quantum State and Electronic Transport* (Oxford University Press, New York, 2010), p. 552.
- [8] G. Seelig and M. Büttiker, *Phys. Rev. B* **64**, 245313 (2001).
- [9] A. E. Hansen, A. Kristensen, S. Pedersen, C. B. Sørensen, and P. E. Lindelof, *Phys. Rev. B* **64**, 045327 (2001).
- [10] P. Mohanty, E. M. Q. Jariwala, and R. A. Webb, *Phys. Rev. Lett.* **78**, 3366 (1997).

- [11] J. J. Lin and J. P. Bird, *J. Phys.: Condens. Matter* **14**, R501 (2002).
- [12] L. Saminadayar, P. Mohanty, R. A. Webb, P. Degiovanni, and C. Bäuerle, *Phys. E* **40**, 12 (2007).
- [13] M. Wilkens, *Phys. Rev. Lett.* **72**, 5 (1994).
- [14] G. Spavieri, *Phys. Rev. Lett.* **82**, 3932 (1999).
- [15] A. V. Chaplik, *JETP Lett.* **62**, 900 (1995).
- [16] A. B. Kalameitsev, V. M. Kovalev, and A. O. Govorov, *JETP Lett.* **68**, 669 (1998).
- [17] R. A. Römer and M. E. Raikh, *Phys. Rev. B* **62**, 7045 (2000).
- [18] A. O. Govorov, S. E. Ulloa, K. Karrai, and R. J. Warburton, *Phys. Rev. B* **66**, 081309(R) (2002).
- [19] V. M. Fomin, *Physics of Quantum Rings* (Springer, Berlin, 2014).
- [20] L. Schweidenback, T. Ali, A. H. Russ, J. R. Murphy, A. N. Cartwright, A. Petrou, C. H. Li, M. K. Yakes, G. Kioseoglou, B. T. Jonker, and A. Govorov, *Phys. Rev. B* **85**, 245310 (2012).
- [21] D. K. Ferry, S. M. Goodnick, and J. Bird, in *Transport in Nanostructures* (Cambridge University Press, New York, 2009), p. 670.
- [22] I. V. Lerner, B. L. L. Altshuler, and Y. Gefen, *Fundamental Problems of Mesoscopic Physics: Interactions and Decoherence* (Springer, New York, 2004).
- [23] Y. Murayama, in *Mesoscopic Systems* (Wiley-VCH, Weinheim, 2001), p. 255.
- [24] For type-II excitons that we study here, the Coloumb interaction is essential and cannot be considered small; thus, the case of weak confinement, according to classification by Ref. [18], is applied here. In this case, only one AB peak is expected. See also the discussion in Sec. III.
- [25] A. Benoît, D. Mailly, P. Perrier, and P. Nedellec, *Superlatt. Microstruct.* **11**, 313 (1992).
- [26] F. Pierre and N. O. Birge, *Phys. Rev. Lett.* **89**, 206804 (2002).
- [27] P. Mohanty and R. A. Webb, *Phys. Rev. Lett.* **91**, 066604 (2003).
- [28] Y. Gu, I. L. Kuskovsky, M. van der Voort, G. F. Neumark, X. Zhou, and M. C. Tamargo, *Phys. Rev. B* **71**, 045340 (2005).
- [29] I. L. Kuskovsky, W. MacDonald, A. O. Govorov, L. Mourokh, X. Wei, M. C. Tamargo, M. Tadic, and F. M. Peeters, *Phys. Rev. B* **76**, 035342 (2007).
- [30] B. Roy, H. Ji, S. Dhomkar, F. J. Cadieu, L. Peng, R. Moug, M. C. Tamargo, Y. Kim, D. Smirnov, and I. L. Kuskovsky, *Phys. Rev. B* **86**, 165310 (2012).
- [31] S. Dhomkar, U. Manna, I. C. Noyan, M. C. Tamargo, and I. L. Kuskovsky, *Appl. Phys. Lett.* **103**, 181905 (2013).
- [32] S. Dhomkar, N. Vaxelaire, H. Ji, V. Shuvayev, M. C. Tamargo, I. L. Kuskovsky, and I. C. Noyan, *Appl. Phys. Lett.* **107**, 251905 (2015).
- [33] H. Ji, B. Roy, S. Dhomkar, R. T. Moug, M. C. Tamargo, A. Wang, and I. L. Kuskovsky, *J. Electron. Mater.* **42**, 3297 (2013).
- [34] B. Roy, H. Ji, S. Dhomkar, F. J. Cadieu, L. Peng, R. Moug, M. C. Tamargo, and I. L. Kuskovsky, *Appl. Phys. Lett.* **100**, 213114 (2012).
- [35] Y. Kim, Y. Ma, A. A. Imambekov, N. G. Kalugin, A. Lombardo, A. C. Ferrari, J. Kono, and D. Smirnov, *Phys. Rev. B* **85**, 121403(R) (2012).
- [36] I. R. Sellers, I. L. Kuskovsky, A. O. Govorov, and B. D. McCombe, in *Physics of Quantum Rings*, edited by V. Fomin (Springer, Berlin, 2014), p. 487.
- [37] H. Ji, S. Dhomkar, B. Roy, V. Shuvayev, V. Deligiannakis, M. C. Tamargo, J. Ludwig, D. Smirnov, A. Wang, and I. L. Kuskovsky, *J. Appl. Phys.* **116**, 164308 (2014).
- [38] S. L. Ren, J. J. Heremans, C. K. Gaspe, S. Vijayaragunathan, T. D. Mishima, and M. B. Santos, *J. Phys.: Condens. Matter* **25**, 435301 (2013).
- [39] M. Y. Reizer, *Phys. Rev. B* **40**, 5411 (1989).
- [40] P. C. Kwok, *Phys. Rev.* **149**, 666 (1966).
- [41] P. Borri, W. Langbein, U. Woggon, V. Stavarache, D. Reuter, and A. D. Wieck, *Phys. Rev. B* **71**, 115328 (2005).
- [42] B. Krummheuer, V. M. Axt, and T. Kuhn, *Phys. Rev. B* **65**, 195313 (2002).